The Dynamics of the Structure of Composite Electrodes during their Operation in Lithium-Ion Batteries

*Thimo Brendel, Manfred Janzen, Marcus Müller, Werner Bauer, Dominik Kramer, and Reiner Mönig**

Mechanical and electrochemical experiments are used to infer changes in composite electrodes during cell operation. Macroscopic stress levels are determined by operando substrate curvature measurements of $LiFePO_4$ (LFP) electrodes containing different types of binders. A reduction in the stress oscillation within a few cycles indicates that the benefits of calendering can be quickly diminished due to structural changes in the electrode. The use of a relatively stiff PAA binder allows for detailed observations of the phase transition during (de)lithiation of LFP, while softer, more viscous binders lead to significantly reduced and blurred macroscopic stresses. To separate mechanical from electrochemical contributions to the electrode mechanics, electrodes are tested with a stress-controlled compression setup, which mimics the macroscopic stress states during electrochemical cycling. This experiment reveals differences in the evolution of strain and electrode resistance, which are consequences of different particle rearrangement processes. Their motion is linked to the mechanical properties of the binder, which highlights its decisive role in the resulting mechanical and time-dependent properties of composite electrodes. The results of this work demonstrate that composite electrodes cannot be considered stationary during operation. Electrodes structurally change and develop towards "steady-state" configurations depending on the operating conditions and the externally imposed load.

1. Introduction

Rechargeable batteries, especially lithium-ion batteries (LIBs), are set to play a major role in the transition from a fossil-based to a sustainable energy infrastructure. Due to the cost of refinement and the limited availability of some raw materials, LIBs should be used as long as possible, once they have been manufactured. Their end of life is often defined by a certain degree of degradation, which can be seen by changes in their electronic and electrochemical properties. For example, this can be the rise of internal resistance or the fade of capacity. The degradation of LIBs can be attributed to chemical and mechanical causes. Changing stresses in the electrodes are assumed to have a significant impact.[1] Electrochemical processes affect the structure of active material particles.[2] Mechanical stresses act on transport paths, i.e., the electrochemically inactive components, as well as on active particles, where they for example, affect phase transitions.[3–5] Generally, stresses in composite electrodes arise as a consequence of volume expansions of the active material and affect the performance and reliability of the electrode. Often, these reversible mechanical stresses are described as the "breathing" of cells. The reversibility of the volume change strongly depends on the active material. For example, silicon-based electrode materials experience large volume changes that are not necessarily reversible.[6] The situation is different for the conventional electrode materials such as graphite, lithium iron phosphate (LFP), and NMC, where the active material is mechanically reversible to a very large extent. Here, the structure of the electrode, including carbon black and binder and its mechanical properties are of interest. So far, deformation of the electrode structure has often been considered to be an elastic and reversible process. Since composite electrodes are multiparticle systems that contain polymeric binders, which are viscous materials,[7] it is not obvious how far the deformation of electrodes can be considered reversible in particular during extended cycling.

In this experimental study, we determine the mechanical stresses within LFP based composite cathodes containing different binder materials that arise upon electrochemical cycling. Furthermore, the observed stresses due to repetitive cycling are replicated in a purely mechanical experiment to gain further insights into the rearrangement processes within the electrodes. In this experiment, individual electrode sheets are cycled mechanically to exclude electrochemical effects that would alter the active material. This enables the detailed observation of the mechanics of the electrode and its

T. Brendel, M. Janzen, M. Müller, W. Bauer, D. Kramer, R. Mönig
Institute for Applied Materials
Karlsruhe Institute of Technology
Hermann-von-Helmholtz-Platz 1, Karlsruhe, Eggenstein-Leopoldshafen
76344, Germany
E-mail: reiner.moenig@kit.edu

The ORCID identification number(s) for the author(s) of this article can be found under https://doi.org/10.1002/ente.202500106.

consequences on the electronic conduction pathways through the electrode composite.

For the determination of stresses during cycling, operando substrate curvature measurements are used. This technique has already been used for monitoring the stress evolution in composite electrodes.[8–10] The macroscopic mechanical stress originates from volume changes of the active material, here the LFP particles. In the LFP, lattice sites are occupied by lithium ions,[11] which can be removed. The intercalation and deintercalation of lithium ions lead to an expansion and a contraction of the particle. This results in stresses within a composite battery electrode due to the interconnections between the electrode particles, including carbon black and binder. Denser electrodes with more contacts between their particles can be obtained by calendering and develop higher macroscopic stresses. It should be noted that the stresses at the level of the electrode and inside the active particles are vastly different. For example, the evolving average stress in composite electrodes based on LFP as obtained by Janzen et al.[12] is about two to three orders of magnitude lower compared to the calculated stress within the active material particles.[13,14]

After the stresses in the electrodes are measured in a commercial electrolyte, dry samples from the same electrode sheets are tested in the mechanical compression setup, which replicates these stresses. With this setup, experiments can be performed reliably on individual electrode layers even at low stresses, in contrast to most mechanical measurements in the literature, which rely on stacks of electrodes to amplify the observable deformations or are performed at much higher levels of stress.[15–18]

Based on the results of both measurement techniques, it becomes evident that the structure of composite electrodes is not fully reversible and that it evolves during cycling. The recorded electrochemical, mechanical, and resistance data are analyzed to infer structural changes in the electrode during operation. Although details of the processes depend on the specific composition (e.g., binder material with vastly different mechanical behavior[19]) of the electrode, the focus of this report is on general trends that are independent of the binder material and are active in commonly used composite electrodes.

2. Experimental Section

Macroscopic stress levels of cathodes with different binder materials and amounts were determined by the operando substrate curvature method. In bilayer systems, where a film is rigidly attached to a substrate, force and momentum balances govern the curvature of the bilayer. For the case that the film thickness is much smaller than the thickness of the substrate, the radius of curvature is directly proportional to the stress in the film.[20] The curvature can be measured with very high sensitivity by laser triangulation. This technique can also be used for battery electrodes to measure or estimate the stress in the electrode during cycling.[8] Here, we use the same setup and also glue our conventional battery electrodes with the aluminum current collector onto a glass cantilever that acts as our substrate. Cathodes containing Li_xFePO_4 particles as active material were fully delithiated and lithiated (x from 1 to 0 and back) at a rate of C/10. The electrodes were held at 2.9 V for 2 h to ensure full lithiation prior to testing. The electrolyte (LP30) was purchased from Sigma Aldrich, consisting of 1 M $LiPF_6$ in ethylene carbonate and dimethyl carbonate (1:1). The electrodes were prepared by dispersing LFP (SC-P2, Süd-Chemie AG) with various amounts of carbon black (CB, Super C65, Imerys) and various binder types in a dissolver mixer using N-Methyl-2-pyrrolidone (NMP) or H_2O as a solvent. NMP was applied in combination with polyvinylidene fluoride binder (PVDF, Kynar HSV900, Arkema), while H_2O was applied for carboxymethyl cellulose (CMC, CRT 2000 PA), polyacrylic acid (PAA, 1.25 Mg mol^{-1}), and latex binder (TRD, TRD202A, JSR Micro). Detailed data of the LFP active material are shown in the supplement (Table S1, Supporting Information). After homogenization, the cathode slurries were coated onto aluminum foil (20 μm thickness) using a laboratory coater with in-line drying (KTF-S, Mathis). The compositions of the different electrodes with their names are listed in **Table 1**. Electrodes were available both as calendered and uncalendered sheets. Scanning electron miroscopy (SEM) images of FP-5PVDF and FP-PAA electrodes in the uncalendered state are provided in **Figure 1**.

The maximum stress range (the difference between minimum and maximum stress during cycling) obtained from the

Table 1. Composition of the LiFePO$_4$ electrodes and the thickness and porosity of the coating for the calendered (cal.) and uncalendered (uncal.) electrodes. The electrodes are named after their majority binder component.

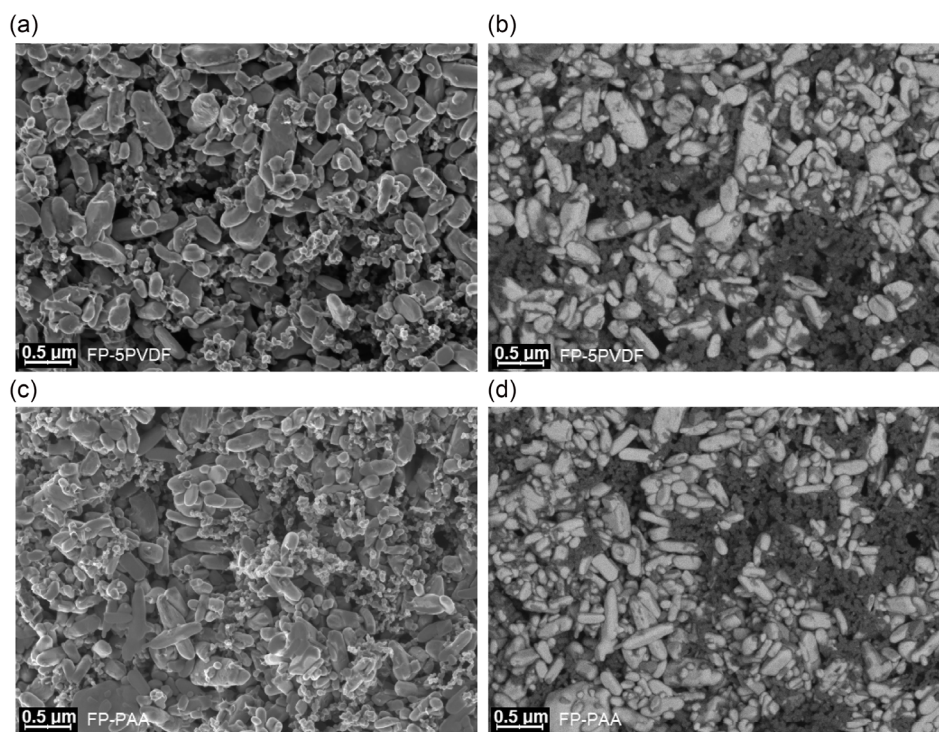| Name of electrode		FP-5PVDF	FP-7.5PVDF	FP-10PVDF	FP-CMC	FP-TRD	FP-PAA
Weight percent in %	LFP	85	85	85	87.7	87.0	87.0
	CB	10	7.5	5	8.8	8.7	8.7
	PVDF	5	7.5	10	0	0	0
	CMC	0	0	0	2.6	1.74	0
	TRD	0	0	0	0.9	2.6	1.7
	PAA	0	0	0	0	0	2.6
Thickness in μm	uncal.	82.5	90.0	83.8	50.3	60.5	43.2
	cal.	69	–	60.1	48.1	50.7	38.9
Porosity in %	uncal.	64.6	64.3	63.9	49.4	64.5	58.1
	cal.	53.3	–	43.3	47.3	56.9	49.4
Measured capacity in mAh cm^{-2}		1.48	–	1.54	0.98	0.71	0.95

Figure 1. SEM images of pristine electrodes. a,b) are from a FP-5PVDF electrode, c,d) are from a FP-PAA sample. a,c) are images recorded with an InLens electron detector showing the morphology. b,d) show the same locations imaged with an in-column energy selective backscatter detector. In these images, the ceramic active material appears bright and carbon-rich spots like the particles of conductive carbon appear dark.

operando substrate curvature experiments can only be regarded as an estimated value, as it contains some sources of error: The electrochemical active layer is not of infinitesimal thickness, as required by Stoney's equation. Further complication arises since it is attached to the substrate via additional layers (current collector and glue). This multilayer problem cannot be easily solved analytically. Therefore, finite element simulations are used to introduce a correction factor to Stoney's equation.[8] The mechanical properties of the layers and the calculated correction factors are stated in the supplement (Table S2, Supporting Information). Compared to Stoney's equation for thin films, the estimated radii of curvature of the multilayers are larger, depending on the electrode thickness and glue, by a factor between 1.34 and 2.3. Another error is due to the expansion and contraction of the electrode during cycling, which is not considered. For these reasons, the axes in the diagrams are labeled with "estimated stress". In the substrate curvature experiment, the electrode is free to expand perpendicular to the substrate and the current collector and the equibiaxial stress that forms during cell operation is recorded.

The stress range estimated from the experimental data was used as an input parameter for a self-constructed stress-controlled compression setup. A schematic is shown in **Figure 2**. Dry cathode samples are mechanically tested under ambient conditions without the presence of electrochemical effects or an electrolyte. In the setup, single or stacked electrodes are placed onto a raised circular region of the bottom plate with a well-defined area (113.1 mm^2) and are compressed by a flat top plate. A defined force is applied
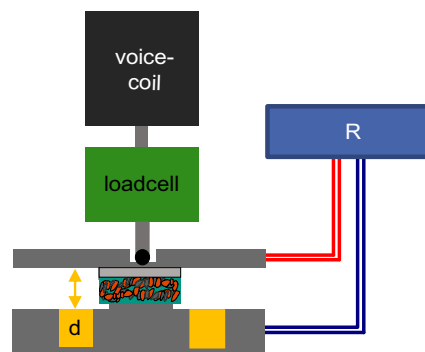

Figure 2. Schematic of the mechanical compression setup. An electrode is placed on the raised area of the bottom plate. Force is applied by a current-controlled voice-coil actuator. The measurement of the force is performed by a load cell, the thickness is measured by three capacitive sensors (d), and the resistance by a 4-wire resistance meter (R).

from above by a current-controlled voice-coil actuator with an added load cell (50–1450 kPa). The top plate is connected to the actuator via a pivot joint, which enables tilting of the top plate in two dimensions. We assume that the externally applied vertical force causes a significant hydrostatic stress component in the film due to numerous redirections of the force at the particle contacts and the presence of the laterally constraining current collector. The electrochemically inactive components of the electrode therefore may experience stress levels that are not vastly different from

2500106 (3 of 11)

**ADVANCED
SCIENCE NEWS**

www.advancedsciencenews.com

Energy Technology
Generation, Conversion, Storage, Distribution

www.entechnol.de

the ones during electrochemical cycling, where the forces originate from the active particles. This assumption is supported by simulation results on the evolving stress state due to uniaxial stress application to granular media.[21,22] Based on these considerations, similar mechanically induced changes to the electrode morphology may be expected to occur. The thickness of the electrode was measured by three high-resolution capacitive sensors in a triangular arrangement. This configuration enables a reliable measurement of the total electrode thickness as well as the detection of tilting of the top plate caused by a nonuniform compression behavior of the electrodes. The evolution of conductivity was obtained by a 4-point resistance measurement between the bottom plate and the top plate. To mimic the conditions during battery operation and to reveal the impact of rate on the change of morphology, load rates between $2.5\,kPa\,s^{-1}$ and $100\,kPa\,s^{-1}$ (time for a full cycle from 1200 to 30 s) were used.

3. Results and Discussion

3.1. Mechanical Stresses during Lithiation and Delithiation for Different Binder Materials

The stresses measured during lithiation and delithiation in **Figure 3** show changes in the range of hundreds of kPa depending on the electrode composition. These stresses at the level of the electrode are dramatically lower compared to those that are expected to develop inside the active material. In simulations, stresses in the active material arise that are on the order of GPa.[13,23] This discrepancy can be explained by the fact that electrochemistry and the associated mechanical forces (differences in lattice expansion due to concentration gradients or the coexistence of phases with different lattice parameters) are present only inside the active material. The porous and compliant composite electrode only responds (kPa stresses) to the volume changes of the highly stressed electrochemically active particles (GPa stresses). The binder plays a key role, since it interconnects the active material particles within the composite electrode and has to adapt to their volume changes.

Since all tested electrodes consist of the same active material and have similar weight fractions (85.0 wt% to 87.7 wt%), the generation of stress in the electrodes is expected to be similar for all samples. The observed differences in the resulting macroscopic stress in the electrodes are therefore suggested to be mostly caused by different material properties of the binders. As depicted in Figure 3, the change in the binder material does not impact the general shape of the stress curve. Both electrodes with CMC (a) or PAA (b) binder show a characteristic stress jump at the beginning of lithium extraction, although to a different extent. This is followed by a relatively linear increase as soon as the voltage plateau of the LFP active material is reached. A linear dependence of lithiation and stress on the voltage plateau can be explained by the different volumes of the lithiated (LFP) and unlithiated (FP) phases and the linear change of their ratio during galvanostatic charge/discharge. The unit cell volume of LFP is 6.7 % larger than that of FP, and depending on the state of charge, different phase fractions and therefore mechanical stresses are present in the electrode.[12] The linear stress dependence, as well as different initial stress jumps, were also observed for other binder materials, as depicted in the supplement (Figure S1, Supporting Information). At the beginning of the lithiation, when moving away from $x = 0$, the shape of the stress curves of the investigated electrodes differs. FP-PAA shows the most noticeable deviation from the otherwise mostly linear stress decline in the form of a small stress dip consisting of a short decrease, a minimum, and a very small rise. This is the
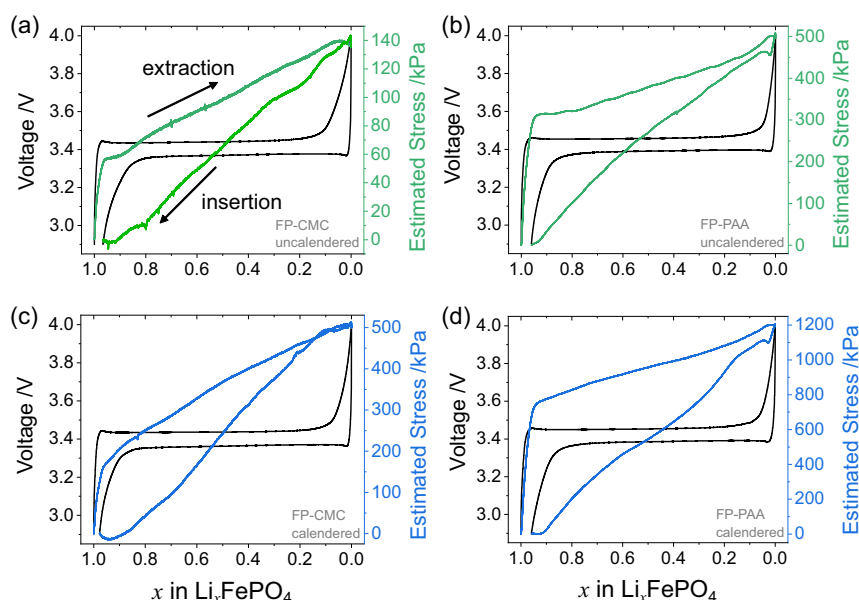

Figure 3. Electrochemical data (black) and mechanical stress (green/blue) of galvanostatic cycles with C/10 for FP-CMC (left side: a,c) and FP-PAA (right side: b,d) composite electrodes. The depicted cycles in a,b) are obtained from uncalendered electrodes (green), while c,d) show measurements of calendered electrodes (blue). Please note the different scales on the vertical stress axes. Data for other binder materials can be found in Figure S1, Supporting Information.

case for both uncalendered and calendered samples. The decrease with a large slope is probably linked to the lithium uptake of a solid solution within the FP phase. The subsequent minimum may be correlated to the nucleation of the LFP phase within the FP particles. The small local minimum is also present in the voltage. In electrochemistry, this is often explained by the energy needed to overcome the nucleation barrier and to start the nucleation process.[24,25] To our knowledge, this detailed correlation between electrochemical and mechanical processes has not been reported in the literature. The high stiffness and low viscosity of PAA allow even subtle mechanical processes to be detected in the macroscopic stress data. Calendering increases the stress range and changes the extent of the hysteresis in all cases, but does not introduce fundamentally new features to the stress curves.

The binder joints between the active material particles may be understood as viscoelastic elements. Soft and viscous binders lead to low electrode stresses and blurred mechanical effects during cycling, whereas stiff and elastic binders attenuate the stresses less. The latter results in higher macroscopic stress levels and stress data exhibiting more details. For the investigation of mechanical processes within active materials, we recommend the use of stiff binders to make the changes at the particle level discernible at the macroscopic level of the electrode. For fabrication reasons, the FP-CMC and FP-TRD electrodes consist of the same two binder materials but with different weight fractions. Here, the binder is labeled with the name of the polymer in the majority. A change in the ratio results in a stress increase by a factor of about three going from FP-TRD to FP-CMC (Figure S1, Supporting Information). This demonstrates that the mixing of binder materials enables tuning of the mechanical properties of the composite electrode.

Besides the material, the total amount of binder can be varied, for example, FP-5PVDF and FP-10PVDF in Figure S1, Supporting Information. Presumably, more binder results in the generation of more and larger binder joints, which stiffen the electrode. Such a stiffening seems to be also present in electrodes densified by calendering. Although FP-TRD and FP-5PVDF electrodes show similar stress ranges in the uncalendered state, significant differences are present after calendering, despite comparable densification. This indicates that the stiffening of the electrodes is not simply linked to the reduction of the thickness of the coating but also to the individual mechanical properties of the binder.

3.2. Evolution of the Stress Range

Cycling of composite electrodes changes their stress state due to repeated uptake and release of lithium ions. The resulting macroscopic stress is shown in **Figure 4**a for a calendered LFP electrode with PAA binder, plotted against the lithium content. PAA is chosen as an example similar trends exist for the electrodes with other binder materials (Figure S1, Supporting Information). The associated charge capacity of cycle two was used to estimate the lithiation of all other cycles shown. Although LFP is generally operated at lower potentials compared to other materials like NMC, some initial electrolyte decomposition can take place during the first charging in LP30 (hexafluorophosphate salt). Therefore, charge and stress data of the first cycle are affected[26] and are not used here. The decrease of the maximum estimated stress and of the area of the hysteresis upon cycling is pronounced during the first few cycles (cycles 2–4) and is followed by a weaker reduction (cycles 5–22), which can be seen by the blue curve in Figure 2b. In cycle 22, the observed stress range was only about 500 kPa. This roughly agrees with the stress range of an uncalendered electrode of the same material (Figure 3b). In the substrate curvature experiment, the electrode is immersed in the liquid electrolyte, and no clamping perpendicular to the current collector is present. Cycling with this boundary condition changes the electrode and at least partially relieves the stresses and the structural changes that were introduced during calendering, where the electrode was compacted by rolling. Despite the reduction of the amplitude, the characteristic features of the curves are still visible at later cycles. The initial spike of the stress at high lithiation ($1.0 > x > 0.95$) is reduced in its amplitude and followed by a linear stress increase during the delithiation process in all cases. The dip at the beginning of the lithiation process becomes less pronounced but does not vanish. In Figure 4b, the charge capacity drops by ~3% within 20 days. The experiments were performed in an operando cell with limited reliability. Here, we assume that this small decline in charge capacity does not have a significant impact on the observed stress evolution. This may be justified because the capacity reduction is only about
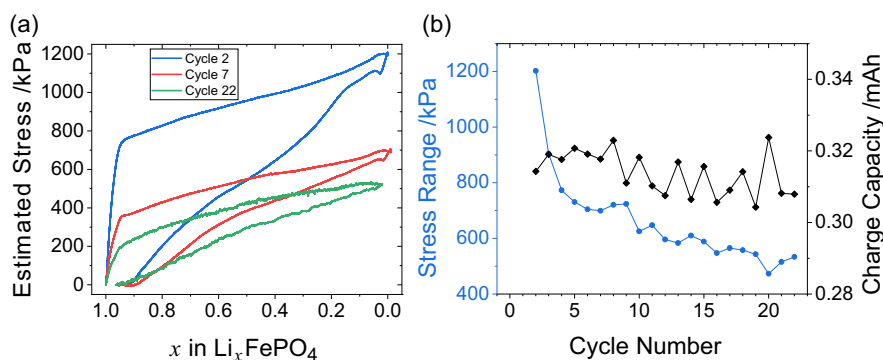

Figure 4. Mechanical and electrochemical data of a calendered FP-PAA electrode during cycling: a) Mechanical stress response during cycling at a rate of C/10. b) Evolution of the mechanical stress range and the capacity over the course of several cycles. Data for other binder materials can be found in.[27]
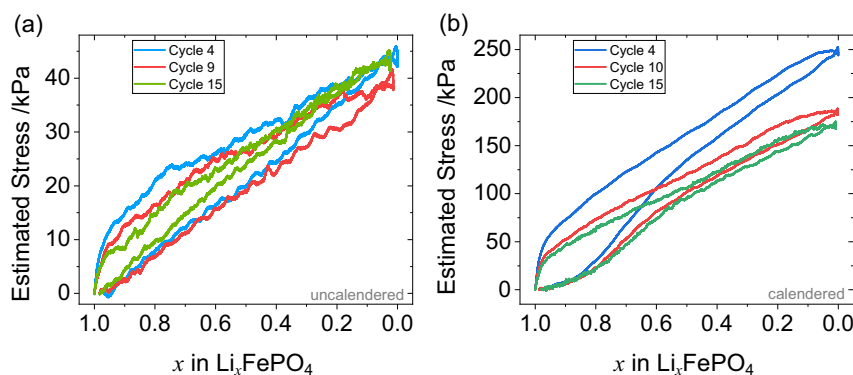
Figure 5. Mechanical stress response of three cycles of an uncalendered a) and a calendered b) FP-5PVDF electrode during galvanostatic cycling with a rate of C/10. Data for other binder materials can be found in.[27]

3% while the stresses are diminished by about 60%. We propose that the reason for the reduction of the stress range is linked to a rearrangement process of the particles (active material, binder, and carbon black), which are in direct contact with each other in the composite coating of the electrode. For example, a reorientation of the nonspherical LFP particles can change the electrode volume and stress response. Also, the movement of binder and carbon black particles away from interconnection points between LFP particles may be responsible for the observed softening of the electrode and the corresponding reduction of the stress range.

The amount of reduction of the stress range depends not only on the binder material but also on the calendering of the electrode. For example, electrodes with PVDF binder material, as depicted in **Figure 5**, have a lower stress range of a maximum 250 kPa (calendered) and 44 kPa (uncalendered). The lower stress range can be explained by the higher compressibility of PVDF due to its lower Young's modulus compared to PAA.[28] Also, when compared to PAA, PVDF is more likely to be moved away from locations of high local stresses due to its lower adhesive strength.[29] For PVDF (Figure 5), the reduction of the stress range in calendered electrodes due to cycling is less pronounced than in electrodes with PAA binder (Figure 4), but the stress still evolves towards the range observed in uncalendered samples. The change of the stress range is most likely accompanied by changes in the electronic transport paths within the electrode. Therefore, it seems reasonable to assume that the intended effects of calendering, such as the reduction of porosity and the improvement of electrical contacts, are partly reversed by the structural evolution of the electrode during cycling. For uncalendered electrodes, no significant reduction is observed during cycling. Here, the volume changes of the active material apparently only lead to reversible elastic deformation of the binder and the resulting stresses are not high enough to force an irreversible movement of particles.

The stress data in Figure 5 contains fluctuations. They are much larger than the resolution of the measurement technique and originate from the electrode itself. We interpret the fluctuations as disruptive local events in the electrode corresponding to localized displacements of particles. In particular, in loosely packed electrodes, elastic energy may accumulate until yielding

in the binder occurs. The sensitivity of our curvature measurement is very high, and we believe that even the fracture of a stressed individual binder bridge is detectable and can contribute to the noise in the data. In the measurements, these sudden local yielding events may be dampened by the viscosity of the binder so that instead of a sawtooth profile, wavy stress oscillations are found. The smaller the number of binder bridges under load, the more discrete these events are. In calendered electrodes, many binder bridges are under load, and the detection of individual events may not be possible in the measured average stress of the electrode.

3.3. Compressive Behavior of Composite Electrodes

Changes in the particle configuration and their consequences on the electron transport paths are investigated by a purely mechanical experiment. Dry electrodes are compressed under controlled stress and displacement, and resistivity of the electrode is measured. Especially the impact on the electrode resistance can hardly be measured precisely within an operational cell. In addition to the mechanical effects, chemical changes in the active material influence the transport paths and may mask the impact of the particle rearrangements. In the experiments, a similar stress range as obtained from the electrochemical experiments is used to mechanically load the electrode samples with the aim of replicating the mechanical effects during lithiation and delithiation. The data of these experiments solely contain compressive stresses. In the following, they are plotted without the commonly used negative sign.

Individual mechanical cycles are displayed exemplarily for FP-PAA and FP-5PVDF electrodes in **Figure 6**. Data for the other binder materials can be found in the supplement (Figure S2, Supporting Information). For all mechanical cycles, stress is applied and released linearly, very similar to what was observed during electrochemical cycling across the voltage plateau. A rate of $10\,\mathrm{kPa\,s^{-1}}$ was used. The maximum stress reaches 1450 kPa, while the minimum stress is kept at 50 kPa to prevent unwanted movement or bending of the electrodes and to retain electrical contact with the surfaces of the electrodes during unloading.

All samples show similar qualitative results during the mechanical compression cycles, but with quantitative differences. During
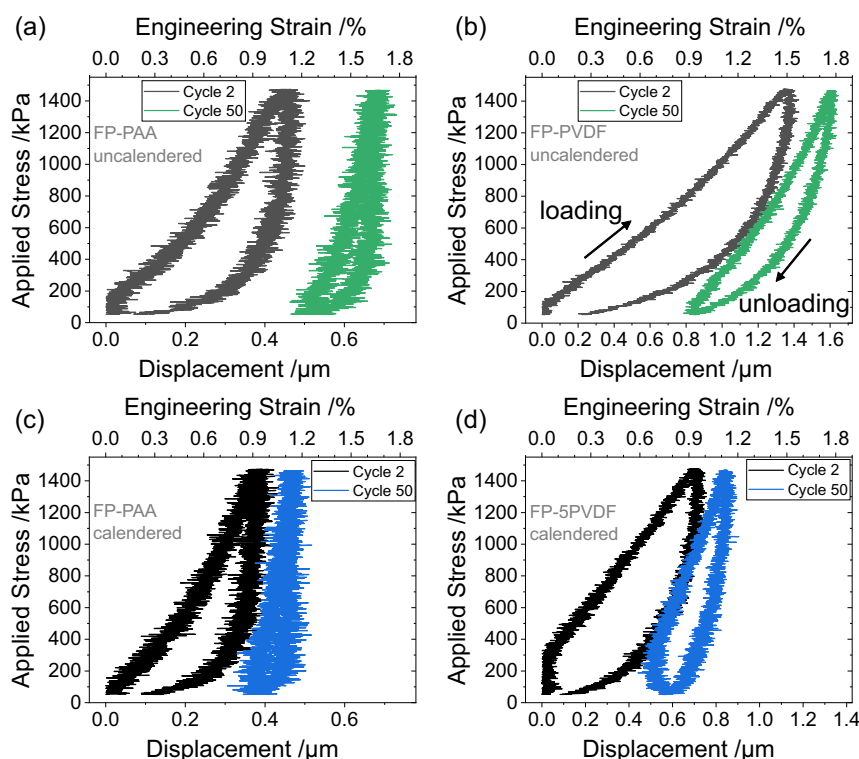
ADVANCED
SCIENCE NEWS
www.advancedsciencenews.com

Energy Technology
Generation, Conversion, Storage, Distribution
www.entechnol.de

Figure 6. Displacement and strain of two different compression cycles of FP-PAA electrodes (left side) and FP-5PVDF electrodes (right side) at a stress rate of 10 kPa s^{-1}. For the experiments of a,b) uncalendered electrodes are used (green). The data in c,d) are obtained from calendered electrodes (blue).

the first cycles, the electrode FP-5PVDF with a compliant binder shows about 40% larger strain compared to FP-PAA. This trend is in good agreement with the different elastic moduli of PVDF and PAA as determined by colloidal probe atomic force microscopy at 1.4 and 3.3 GPa.[28] Besides selecting different binder materials, the fraction of the binder can be changed to tune the stiffness of the electrode. For uncalendered electrodes, the engineering strain is reduced from 1.5 % to 0.7 % when the content of PVDF is doubled. In the case of calendered electrodes, the strain changes from 0.9 % to 0.6 %. Presumably, more and/or larger binder joints are established in samples with higher binder content. Calendering leads to a deformation and shortening of binder bridges and to a redistribution of binder material into the pore space. We expect that in such dense electrodes direct contacts between active material particles are more frequent and therefore the stiffness is less affected by the binder content and type.

With all electrodes, a stiffening occurs during mechanical cycling. Figure 6 shows reduced displacements and hysteresis areas after 50 cycles. Also, here a rearrangement of the electrode might lead to an increased number of contacts between active material particles. In calendering, electrodes quickly densify by the application of a high external force. A similar densification may occur during battery operation in compressed cells when small forces are applied repetitively. Calendered electrodes are already densified therefore, mechanical cycling over 50 cycles increases the stiffness less than in the case of uncalendered electrodes. The observed cyclic calendering during cell operation might be usable in real cells during operation to tune or

optimized their electrode structure. Effects of calendering using a roll-based calender can be achieved already at low stresses.[30] The cyclic application of low stresses during operation of a clamped cell is suggested to amplify the changes of the electrode structure leading to thinner electrodes with reduced porosity (**Figure 7** and Figure S3, Supporting Information).

The path of loading and unloading shows a clear hysteresis effect. The enclosed area is significantly smaller for calendered electrodes, just as during electrochemical cycling in Figure 3. The hysteresis shows the dissipated energy of a process. Here, this is most likely the rearrangement of particles and the heat generated by the viscoelastic deformation of the binder. The reorientation of nonspherical particles due to stress was addressed in simulations[31] and considered to be responsible for irreversible deformation, causing changes in the electrode thickness after loading and subsequent unloading. This might also lead to hysteretic stress—strain behavior. However, in the experiments, the hysteresis persists even after multiple cycles; therefore reorientation of nonspherical particles cannot be the only explanation for a hysteresis. Presumably, in addition to particle reorientation, energy is lost during the viscoelastic deformation of the binder.[32,33] In contrast to the reorientation of particles, this mechanism is still active in later cycles. The decrease in hysteresis (especially after cycling) is comparable to results from the operando substrate curvature method, indicating that a stabilization process of the electrode takes place. After several cycles, the dissipated energy (hysteresis area) is reduced, which might be explained by the ongoing optimization
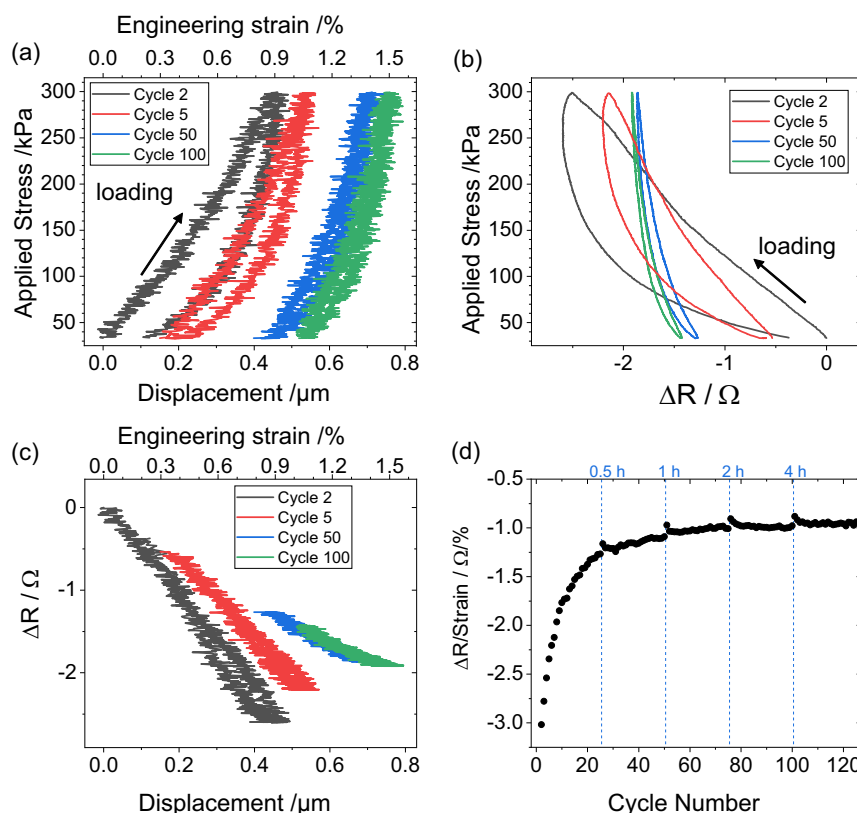
Figure 7. a) Compressive behavior of an uncalendered FP-PAA electrode for different cycle numbers. Resistance change caused by the applied stress b) and resistance versus displacement c). d) change of resistance-strain-dependence over 125 cycles including relaxation breaks marked by blue lines. The results for an uncalendered FP-5PVDF electrode, as well as resistance changes of other electrodes are shown in the supplement (Figure S3, Supporting Information). Data for other binder materials can be found in.[27]

of the electrode structure during cycling. The optimization consists of the reduction of energy losses within individual cycles. This is probably accomplished by the movement of individual particles of the active material away from highly stressed locations into regions where they experience lower stresses, e.g., in the pore space. We suggest that this is an iterative process where the initially highly stressed particles find positions where they experience only low stresses and consequently do not move any further, i.e., the electrode has stabilized. These local peak shaving events would lead to a more homogeneous stress distribution within the electrode structure after several cycles (at a given SOC).

3.4. Evolution of Electrode Mechanics and Resistivity during Cycling and the Impact of the Stress Rate

The structural evolution of the electrode during cycling impacts the conductive pathways. Figure 7 shows the evolution of uncalendered FP-PAA electrodes using a similar stress range as obtained from electrochemical cycling (see Figure 3). Although the stress amplitude in Figure 7a is more than five times lower compared to Figure 6a, the same trends persist, and also here the electrode structurally evolves. Simultaneously with the load, the resistance of the electrode was measured. Before cycle two, the resistance

through the electrode was $8.9\,\Omega$ across an area of $113.1\,mm^2$ at 50 kPa. In the first few cycles in Figure 7b, this resistance oscillates with an amplitude of $\sim 2\,\Omega$ that decreases with cycling to $\sim 0.6\,\Omega$ after 50 cycles. The detailed evolution of the resistance amplitude is given in the supplement (Figure S4b, Supporting Information). The shape of the resistance curves in Figure 7b, including their hysteresis, shows resemblance to the strain data in Figure 7a. While the electrode densifies from cycle to cycle, the amplitude of the resistance reduces strongly, and the mean resistance reduces only slightly. The resistance settles roughly in between the minimum and maximum value obtained in the first few cycles. When the resistance is plotted against the displacement of the electrode, a relatively linear correlation with little hysteresis is found (Figure 7c). This implies that the electrode thickness (strain) has a more direct impact on the resistance of the electrode than the mechanical stress.

In Figure 7c, the resistance oscillates by $\sim 30\%$ while the thickness changes by less than 1%. This very different scaling of both quantities indicates that the resistance is not simply a result of the changing geometry at constant resistivity. We suggest that the resistance is controlled by the changes in the contacts between the carbon black and active material particles in the electrode. Both the displacement and the resistance dependence on stress settle after several cycles. Upon extended cycling, the resistance of the electrode becomes decreasingly dependent on the

electrode thickness. This can be seen by the decreasing slope in Figure 7c. This effect is also apparent in Figure 7b where the resistance beyond 50 cycles depends very little on the applied external stress. In Figure 7d, the slope of the linear dependence between resistivity and strain is plotted for up to 125 cycles. Its changes are most pronounced during the first ~20 cycles.

The different dependence of thickness (strain) and resistivity on the number of cycles indicates that thickness and conductive pathways change differently. Assuming that carbon black controls the resistivity of the electrode, this could mean that carbon black moves – probably together with the binder[34] – differently from the active material particles of the electrode. This is plausible since carbon black particles are small and can be redistributed due to local mechanical stresses, i.e., they may move away from highly stressed regions into regions with lower stress. There, the lower stress amplitudes lead to smaller changes in the contact area of carbon black with its surrounding particles. Hence, the impact of mechanical stress on the electrode resistance becomes lower. The small carbon black particles may move even without significantly affecting the thickness and stiffness of the electrode. Their high mobility is suggested to cause the fast resistance drop within the first few cycles and may also be responsible for resistance changes at a higher number of cycles when the thickness of the electrode has almost settled.

An example of the suggested rearrangement mechanism of the electrode is shown in **Figure 8**. Carbon black particles are significantly smaller than the active material particles (see SEM images of FP-5PVDF and FP-PAA in Figure 1). The electrode before mechanical loading has well-distributed carbon black particles that form an electronic network with several conductive paths.[35] During settling, particles move away from highly compressive regions into more tensile regions, e.g., the pore space. Carbon black particles may move away from stress

concentrations between adjacent active material particles, as shown in Figure 8c. After moving, they will still be in electrical contact with the active particles in their vicinity (Figure 8d) but experience lower forces upon cycling and therefore stay in this position (settling).

The resistivity of the electrode strongly depends on the contact areas between particles, and in particular on the contacts to and between carbon black. Since the contact area between carbon black and active material particles after settling (Figure 8d) varies less during cycling, the electrode resistance becomes less sensitive to stress. In this way, the electrode structure optimizes in response to the applied mechanical load. As a consequence, further rearrangements are less likely and conductive paths only vary little during cycling.

Optimization or self-optimization in this context means changes in the positions of all particles within the electrode. This affects the mechanical stress and the resistivity of the electrode. This process saturates when the boundary conditions do not change between cycles. For example, the electrode used here settles after 20 or 30 cycles (Figure 7d). We expect that in a real cell, continued usage will cause little change to the electrode, but when the boundary conditions change (i.e., stack pressure, voltage window, or rate), the electrode starts over with an optimization, i.e., structural change. At the beginning, there will be increased stress levels and higher electrode resistance. The optimization may have practical consequences: If for example, the utmost power of the cell is needed, precycling with the desired conditions will help to optimize or train the electrode to reduce its electronic resistivity (Figure 7c) to a minimum.

In **Figure 9**, the effect of cycling rate on the adaption of the electrode due to stress is investigated by comparing different rates. The statistical error in the measurements can be observed by comparing neighboring datapoints. Higher rates show more noise because fewer data points are recorded during one oscillation. The trends between the different rates appear to be significant when considering the noise of the data. The relative (normalized) strain amplitude is the relation between the current strain amplitude and the reference strain amplitude recorded in the first cycle. In Figure 9, lower rates lead to larger drops in the amplitude per cycle. This suggests more settling per cycle, which is in agreement with the longer presence of stress in the slower
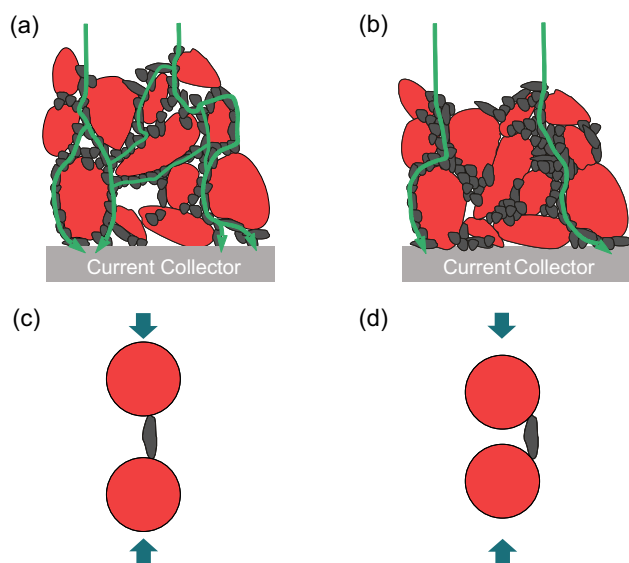

Figure 8. Schematic of the rearrangement of active material particles (red) and carbon black (black) due to varying compressive stress and electron conductive pathways (green). a) Initial electrode structure b) structure after compression. c) Movement of a carbon black particle experiencing high local stress d) towards a location with lower local stress.
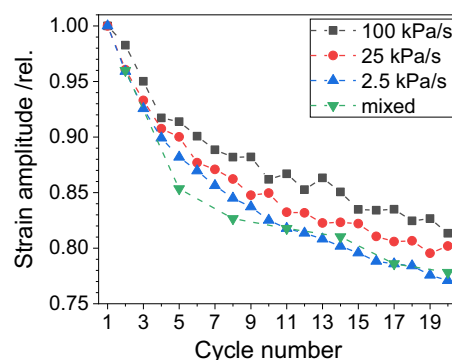

Figure 9. Reduction of the strain amplitude of uncalendered FP-7.5PVDF during mechanical cycling using constant rates of 100, 25, and 2.5 kPa s^{-1}, as well as a mixed rate profile.

**ADVANCED
SCIENCE NEWS**

www.advancedsciencenews.com

Energy Technology
Generation, Conversion, Storage, Distribution

www.entechnol.de

cycles. This demonstrates the strong time dependence of the structural changes of the composite electrode during operation.

The green triangles in Figure 9 are gathered using rate variations. Rates of 100, 25, and $2.5\,kPa\,s^{-1}$ are used in subsequent cycles in regular repetition. Therefore, only every third data point is plotted, which was recorded at $25\,kPa\,s^{-1}$. The reduction in strain amplitude per cycle is comparable to the lowest rate, although the average time per cycle is only 37.5 % of that of the lowest rate. A possible explanation for this faster settlement can be derived when considering the local environments in the electrode. The binder distribution is not homogeneous, and binder bridges of different dimensions exist. The polymeric binder has not only elastic but also viscoelastic properties, where different rates lead to different amounts of deformation. Cycling with a constant rate will repetitively generate similar forces in individual binder bridges. When the rate is varied, the forces in the same bridges will change because of the viscoelasticity and the resulting different time constants of these binder bridges. Following these arguments, it is likely that the settlement process/structure optimization can be tuned by varying the stress rate, i.e., charge and discharge rate during the operation of a cell.

4. Conclusion

During the operation of a battery, the electrodes experience internal mechanical stresses due to volume changes of the active material. These stresses originate from the stiff ceramic material and mainly affect the other components of the electrode. In the composite, they cause structural changes that affect performance and reliability.

In this work, we evaluate the effect of internal and external mechanical stress on a composite electrode similar to the ones in application. Experiments on electrodes are performed in a way that changes in the active material due to electrochemistry are separated from electrical and mechanical effects that are active in the electrode composite: First, electrodes were electrochemically cycled, and the macroscopic stresses in the electrodes were characterized. Second, stresses of similar magnitude were applied to the same electrodes in the dry state and displacement and resistivity were recorded. The second experiment excludes electrochemical processes in the active material and the effects of the electrolyte. This helps to better understand stress-induced changes in the electrode.

In both experiments, cycling causes changes to the electrode that strongly reduce the mechanically stored energy and energy loss per cycle, i.e., hysteresis (Figure 4a and 7a). It is suggested that particles in the electrode move away from regions of high stress towards regions of lower stress, where they remain. This process of local yielding is not time-independent. The data suggests that this is strongly influenced by the viscous flow, including viscoelasticity, of the binder material. This leads to effects that depend on time, cycle number, and rate. Even with the least viscous binder (PAA), the electrode structure is by no means stationary. It changes and relaxes depending on external and internal mechanical loading. External loading corresponds to stack pressure, internal loading is influenced by the cycling conditions, i.e., state of charge, depth of discharge, but also rate. An

example of such an adaption is the cycling of a free-standing electrode in a liquid electrolyte, which partly reverts its densification that was introduced by calendering (Figure 4).

Mechanical effects manifest not only by a change in the electrode structure and geometry, but they also affect the electrochemical performance via changes in the resistive network. Within a cycle, the electrode resistance changes roughly linearly with displacement (Figure 7c). This dependence decreases with cycling and exhibits a different dependence on the number of cycles than the thickness settling of the electrode. The fact that the electrode resistance is not directly related to the geometry of the electrode indicates that changes at the contact points between particles happen and that particles rearrange in the electrode during operation. Our data suggests that the larger active particles rearrange first and change both the resistivity and the thickness of the electrode. The observation that the resistance keeps changing after the electrode has almost settled in thickness can be explained by the motion of the conductive additive. Carbon black particles are small and changes in their distribution hardly alter the electrode thickness. They may be pushed away from highly stressed regions (Figure 8), further reducing the dependence of electrode resistivity on the mechanical strain/stress in later cycles.

In this work, we investigated electrodes with binder polymers with very different mechanical properties (Figure S1 and Figure S2, Supporting Information). On the one hand, all materials show similar qualitative behavior regarding the shape of resistance and displacement during cycling and their evolution upon extended cycling. On the other hand, quantitative differences can be identified regarding the stress amplitude during electrochemical cycling and stiffness during mechanical cycling. Despite very different binder viscosities, all electrodes show time- and cycle number-dependent settling. The stiffest binder PAA has been proven useful for substrate curvature experiments, where an accurate mechanical response of the active material has to be observed. Increased viscosity is expected to introduce failure tolerance and increase the self-repair and self-optimization (settling) capabilities of the electrode structure. Figure S1 and Figure S2, Supporting Information may serve as a first guideline to engineer electrodes with tailored mechanical stresses during operation. The mechanical data presented here consists of experiments on dry electrodes. In contact with an electrolyte, the mechanical properties of the polymeric binders are altered. Nevertheless, similar trends as reported here may be observed.

The results presented clearly show that electrodes should not be considered stationary. They persistently adapt to the prevailing conditions during cycling. In this process, small structural changes affect the mechanics and resistivity of the electrode and alter the electrochemical performance. In the future, accurate models on cell performance and reliability may need to consider the mechanical oscillations during operation and their effect on electrode structure and electronic transport.

Supporting Information

Supporting Information is available from the Wiley Online Library or from the author.

Conflict of Interest

The authors declare no conflict of interest.

Data Availability Statement

The data that support the findings of this study are available from the corresponding author upon reasonable request.

[1] A. Mukhopadhyay, B. W. Sheldon, *Prog. Mater. Sci.* **2014**, *63*, 58.

[2] D. Chen, D. Kramer, R. Mönig, *Electrochim. Acta* **2018**, *259*, 939.

[3] V. A. Sethuraman, M. J. Chon, M. Shimshak, V. Srinivasan, P. R. Guduru, *J. Power Sources* **2010**, *195*, 5062.

[4] B. W. Sheldon, S. K. Soni, X. Xiao, Y. Qi, *Electrochem. Solid-State Lett.* **2012**, *15*, 9.

[5] H. Yang, W. Liang, X. Guo, C.-M. Wang, S. Zhang, *Extreme Mech. Lett.* **2015**, *2*, 1.

[6] A. Al-Obeidi, D. Kramer, S. T. Boles, R. Mönig, C. V. Thompson, *Appl. Phys. Lett.* **2016**, *109*, 071902.

[7] I. M. Ward, J. Sweeney, *Mechanical Properties of Solid Polymers*, John Wiley & Sons, Chichester, UK **2012**.

[8] Z. Choi, D. Kramer, R. Mönig, *J. Power Sources* **2013**, *240*, 245.

[9] S. P. V. Nadimpalli, V. A. Sethuraman, D. P. Abraham, A. F. Bower, P. R. Guduru, *J. Electrochem. Soc.* **2015**, *162*, 2656.

[10] A. Chanda, A. Pakhare, A. Alfadhli, V. A. Sethuraman, S. P. V. Nadimpalli, *J. Power Sources* **2024**, *609*, 234678.

[11] A. K. Padhi, K. S. Nanjundaswamy, J. B. Goodenough, *J. Electrochem. Soc.* **1997**, *144*, 1188.

[12] M. Janzen, D. Kramer, R. Mönig, *Energy Technol.* **2021**, *9*, 2000867.

[13] T. Zhang, M. Kamlah, *J. Electrochem. Soc.* **2020**, *167*, 020508.

[14] X. Zhang, W. Shyy, A. M. Sastry, *J. Electrochem. Soc.* **2007**, *154*, A910.

[15] W.-J. Lai, M. Y. Ali, J. Pan, *J. Power Sources* **2014**, *245*, 609.

[16] D. Sauerteig, N. Hanselmann, A. Arzberger, H. Reinshagen, S. Ivanov, A. Bund, *J. Power Sources* **2018**, *378*, 235.

[17] Z. Wu, L. Cao, J. Hartig, S. Santhanagopalan, *ECS Trans.* **2017**, *77*, 199.

[18] C. Zhang, J. Xu, L. Cao, Z. Wu, S. Santhanagopalan, *J. Power Sources* **2017**, *357*, 126.

[19] T. Yim, S. J. Choi, Y. N. Jo, T.-H. Kim, K. J. Kim, G. Jeong, Y.-J. Kim, *Electrochimica Acta* **2014**, *136*, 112.

[20] G. G. Stoney, C. A. Parsons, *Proc. R. Soc. Lond. Ser. Contain. Pap. Math. Phys. Character* **1997**, *82*, 172.

[21] F. Radjai, M. Jean, J.-J. Moreau, S. Roux, *Phys. Rev. Lett.* **1996**, *77*, 274.

[22] C. Thornton, D. J. Barnes, *Acta Mech.* **1986**, *64*, 45.

[23] M. Huttin, M. Kamlah, *Appl. Phys. Lett.* **2012**, *101*, 133902.

[24] P. Biswal, S. Stalin, A. Kludze, S. Choudhury, L. A. Archer, *Nano Lett.* **2019**, *19*, 8191.

[25] W. Dreyer, J. Jamnik, C. Guhlke, R. Huth, J. Moškon, M. Gaberšček, *Nat. Mater.* **2010**, *9*, 448.

[26] B. Bal, B. Ozdogru, D. T. Nguyen, Z. Li, V. Murugesan, Ö. Ö. Çapraz, *ACS Appl. Mater. Interfaces* **2023**, *15*, 42449.

[27] M. Janzen, *Mechanical Investigations of Composite Electrodes for Li-Ion Batteries*, Dissertation, Karlsruhe Institute of Technology, KaShe **2025**, https://doi.org/10.5445/IR/1000182052.

[28] Q. D. Nguyen, E.-S. Oh, K.-H. Chung, *Polym. Test.* **2019**, *76*, 245.

[29] Z. Zhang, T. Zeng, Y. Lai, M. Jia, J. Li, *J. Power Sources* **2014**, *247*, 1.

[30] A. C. Ngandjong, T. Lombardo, E. N. Primo, M. Chouchane, A. Shodiev, O. Arcelus, A. A. Franco, *J. Power Sources* **2021**, *485*, 229320.

[31] V. Becker, O. Birkholz, Y. Gan, M. Kamlah, *Energy Technol.* **2021**, *9*, 2000886.

[32] Z. Karkar, D. Guyomard, L. Roué, B. Lestriez, *Electrochim. Acta* **2017**, *258*, 453.

[33] A. Vinogradov, F. Holloway, *Ferroelectrics* **1999**, *226*, 169.

[34] J. Entwistle, R. Ge, K. Pardikar, R. Smith, D. Cumming, *Renew. Sustain. Energy Rev.* **2022**, *166*, 112624.

[35] F. Cadiou, T. Douillard, N. Besnard, B. Lestriez, E. Maire, *J. Electrochem. Soc.* **2020**, *167*, 100521.